HARMONI first light spectroscopy for the ELT: geometrical calibration in the data reduction software

Laure Piqueras, Aurélien Jarno, Louise Friot-Giroux, Thomas Béchet, Javier Piqueras López, Arlette Pécontal-Rousset, Johan Richard, Nicolas Bouché, Niranjan A Thatte, Matthias Tecza

HARMONI – first light spectroscopy for the ELT: Geometrical calibration in the data reduction software

Laure Piqueras*[a], Aurélien Jarno[a], Louise Friot--Giroux[a], Thomas Béchet[a], Javier Piqueras Lopez[b], Arlette Pécontal[a], Johan Richard[a], Nicolas Bouché[a], Niranjan A. Thatte[c], Matthias Tecza[c]
[a]Univ Lyon, Univ Lyon1, Ens de Lyon, CNRS, Centre de Recherche Astrophysique de Lyon UMR5574, F-69230, Saint-Genis-Laval, France;
[b]Centro. de Astrobiologia, CAB, CSIC-INTA, Madrid, Spain;
[c]Univ. Of Oxford, Keble Road, Oxford, United Kingdom;

ABSTRACT

HARMONI is the first light visible and near-IR integral field spectrograph for the ELT. It covers a large spectral range from 450nm to 2450nm with resolving powers from R (≡λ/Δλ) 3500 to 18000 and spatial sampling from 60mas to 4mas. It can operate in two Adaptive Optics modes - SCAO (including a High Contrast capability) and LTAO - or with NOAO. The project is preparing for Final Design Reviews.

HARMONI slices the input light beam in subfields and then into slitlets and rearranges them to obtain spectra on its detectors. The Data Reduction software (DRS) handles calibration and scientific raw data from HARMONI and computes a fully reduced and calibrated science data cube. The challenge is to develop robust methods suitable for each of the 44 scale/band combinations of HARMONI. The geometrical calibration, one of the steps of the DRS, determines the coordinate transformation from detector pixels to wavelength and relative spatial position in the input focal plane. This paper provides a mathematical description of the algorithms involved in the geometrical calibration and presents validations on mock data simulated with the HARMONI Instrument Numerical Model (HINM).

Briefly, to cope with a possible overlap of slitlets, we locate the slitlets using a global fitting method on flat-field exposures. The wavelength solution is computed using arc exposures. To compute the geometrical transformation we choose to use specific masks illuminated with a white continuum lamp. A trace mask exposure provides the transformation along the slitlets. A pinhole mask exposure determines the transformation in the perpendicular direction by fitting the flux within each slitlet.

Keywords: ELT, HARMONI, science software, data reduction, geometrical calibration

1. INTRODUCTION

1.1 The HARMONI instrument

HARMONI [1] is a visible and near-infrared integral field spectrometer (0.45 to 2.45 μm), producing more than 31,000 spectra in a single exposure. The overall wavelength range is split into one visible and ten near-infrared spectral bands, with three resolving power (~3500, ~7000 and ~18000). The visible band uses its four CCD detectors while all near-infrared bands share eight H4RG detectors. The field-of-view of HARMONI is sampled by 204x152 spatial pixels (spaxels) with four spaxel scales (60x30, 20x20, 10x10 and 4x4mas). HARMONI is one of the first-light instruments for the European Extremely Large Telescope (ELT). Thanks to the enormous 39-meter main mirror of the ELT, it will be used to study galaxies in the early Universe and characterize exoplanets in great detail.

HARMONI is a combination of optical systems for real-time atmospheric correction (SCAO and LTAO, [2]) and an integral field spectrograph (IFS, [3]) placed in a cryogenic environment. The cryostat interfaces with the instrument rotator and the AO systems. Within the cryostat, the light is first scaled by the pre-optics sub-system to be suitable for input to the

* laure.piqueras@univ-lyon1.fr

IFU (Integral Field Unit) sub-system. Then, the HARMONI field splitter divides the field of view in 8 subfields. Each subfield is split into 38 mini-slits by the slicer. Each mini-slit is then dispersed by the spectrograph producing a 2D spectrographic image on the detector named a "slitlet".

A Calibration Unit (CU) system reproduces the exit pupil of the telescope and provides uniform white and arc light illumination at the telescope focal plane and over the complete HARMONI field of view. The CU system will also include a set of calibration masks that can be inserted in the telescope focal plane.

The international consortium developing HARMONI is led by the University of Oxford and the UK-ATC in Edinburgh. The project is preparing for Final Design Reviews (FDR).

1.2 The HARMONI science software

The Data Reduction Software (DRS, [4]) reconstructs data cubes from scientific raw data and also compensates for the instrumental signature and the environmental effects (e. g. atmospheric refraction, sky background …). It receives as input the raw science exposures and its associated calibration exposures. As any other ESO data reduction software, the pipeline for HARMONI is split into data-reduction tasks known as recipes. These recipes are developed using ESO-CPL, an ESO toolkit containing a set of ISO-C libraries offering high-level I/O routines to load and play with exposure data and a variety of general-purpose image and signal processing functions [5]. ESO also offers HDRL, the High Level Data Reduction Library, which provides several common astronomical data reduction algorithms for data reduction pipelines [6]. Obviously, the HARMONI DRS shall comply with ESO deliverable quality standards. Thus the delivery package includes all documentation associated to the development, design and tests of the data reduction software and of course all end user documentations.

The HARMONI pipeline is currently being designed at CRAL. Prototypes of algorithms identified as critical will have to be delivered for the FDR. The geometrical calibration is one of them.

As mock data are required in order to test the prototypes, we are developing in parallel to the pipeline, an HARMONI Instrument Numerical Model (HINM, [7]). This tool written in Python simulates the instrument from the optical point of view and creates FITS files similar to the raw exposures that will be provided by HARMONI.

1.3 Geometrical calibration of the data reduction software

The geometrical calibration is split into three recipes which process the calibration data taken during day time to evaluate respectively the location of the spectra on the detector, the wavelength solution and the geometrical transformation. These recipes use results from previous steps regarding the detectors effects and the flat field correction. They take as input different sets of exposures obtained using the calibration unit equipped with different masks covering the science field placed in a virtual focal plane coinciding with the instrument object focal plane (i.e. the telescope focal plane). In a typical calibration sequence, each type of exposures is taken three times; the recipe starts by correcting each raw exposure for the detector systematics and converting it into an electron rate (e-/s) map; then the three maps are collapsed using a sigma clipping mean method available in the HDRL library. The following sections describe the analyses done on these collapsed images (one per detector).
The diversity of the HARMONI configurations requires the development of a challenging algorithm to minimize the number of calibration exposures per configuration.

2. SLITLET LOCATION

The determination of the slitlet location is the first step of the HARMONI geometrical calibration process. It determines where to look for the signal by associating each detector pixel to a slitlet. The 38 slitlets are located by analysing a set of flat exposures acquired with the entire field-of-view illuminated with a continuum lamp as shown on the Figure 1. The algorithm computes 5 polynomials per slitlet: center of the slitlet, left and right edges as a function of the vertical location on the detector, and bottom and top edges as a function of the horizontal location on the detector.

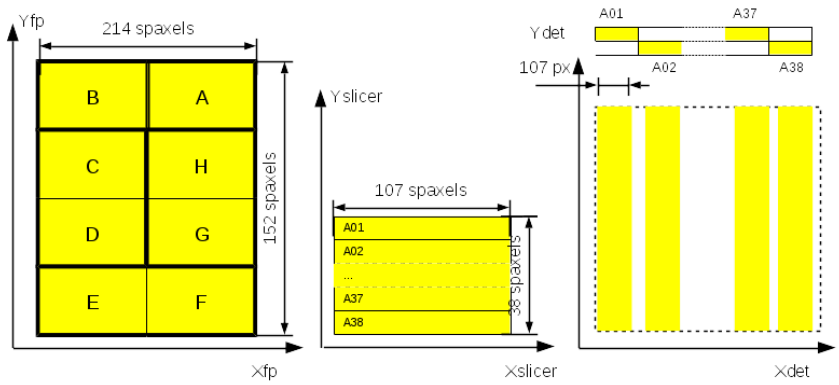

Figure 1. Scheme of a flat exposure through the HARMONI instrument

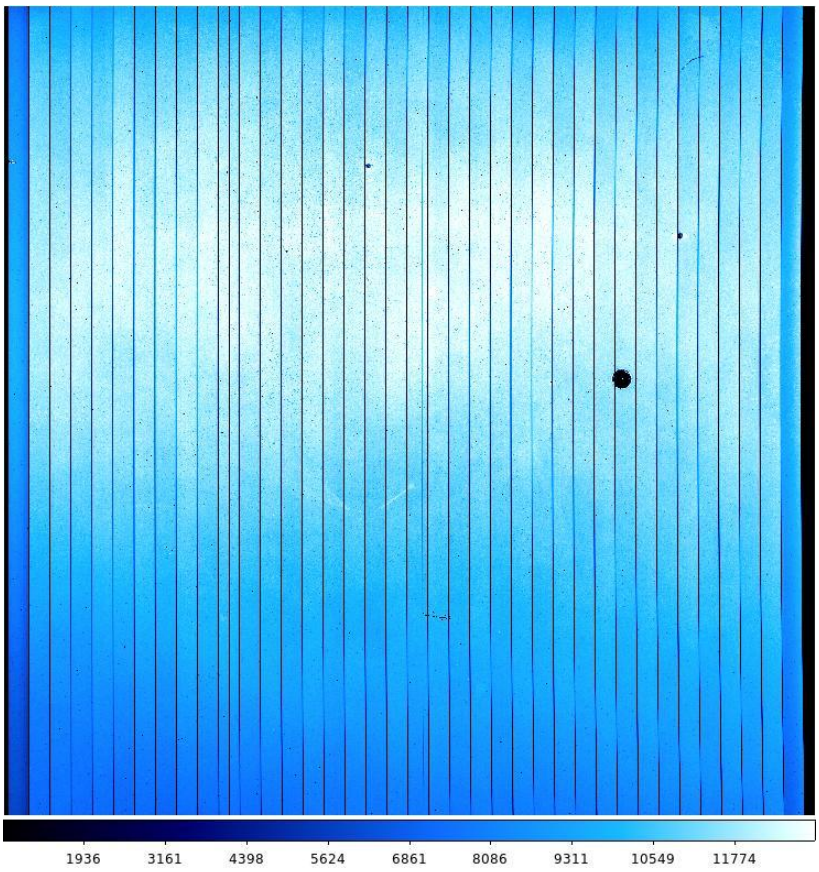

Figure 2. Simulated continuum lamp exposure for one detector in H band (z-scale).

Figure 2 shows a mock flat exposure for one detector generated by the HINM. The continuum lamp is simulated as a black body spectrum with a spatially constant illumination of the field-of-view and with a maximum of 20000 ADUs.
For each detector, the algorithm analyses the flat image row by row and determines the centres and the edges of the 38 slitlets. Because the slitlets could overlap, the process considers the whole detector row in order to detect all slitlet locations at the same time.

The algorithm assumes that the image of each slice can be approached by a top-hat profile convolved by the PSF of the spectrograph. This PSF is approximated by a Gaussian profile. The convolution of a top hat with a Gaussian is defined by the equation (1):

$$I\int_{x-c-\frac{\Delta}{2}}^{x-c+\frac{\Delta}{2}}\frac{1}{\sigma\sqrt{2\pi}}e^{\frac{-t^2}{2\sigma^2}}dt=\frac{I}{2}\left(erf\left(\frac{x-c+\frac{\Delta}{2}}{\sigma\sqrt{2}}\right)-erf\left(\frac{x-c-\frac{\Delta}{2}}{\sigma\sqrt{2}}\right)\right) \quad (1)$$

c is the x-coordinate of the slitlet centre, Δ is the width of the corresponding top-hat and I is the flux amplitude, σ is the standard deviation of the Gaussian profile and $erf(x)=\frac{2}{\sqrt{\pi}}\int_0^x e^{-t^2}dt$ is the error function.

A detector row is approximated by the sum of 38 top-hats (one for each slitlet) convolved by the PSF of the instrument:

$$\sum_{i=1}^{38}\frac{I_i}{2}\left(erf\left(\frac{x-c_i+\frac{\Delta_i}{2}}{\sigma\sqrt{2}}\right)-erf\left(\frac{x-c_i-\frac{\Delta_i}{2}}{\sigma\sqrt{2}}\right)\right) \quad (2)$$

Figure 3 shows a detector row and the corresponding solution solved by least-square minimization. To be more exact, the figure shows an averaged flux value along the x-axis of the 100 neighbouring rows around the central row, because the flux values are averaged around the given detector row in order to decrease the noise effect. To quantify the accuracy of the solution, errors are calculated from the covariance matrix estimated during the least square minimization. Centres of the 38 top-hats (i.e. centres of the slitlets) are determined with an error better than 0.02 pixel for different instrument settings.

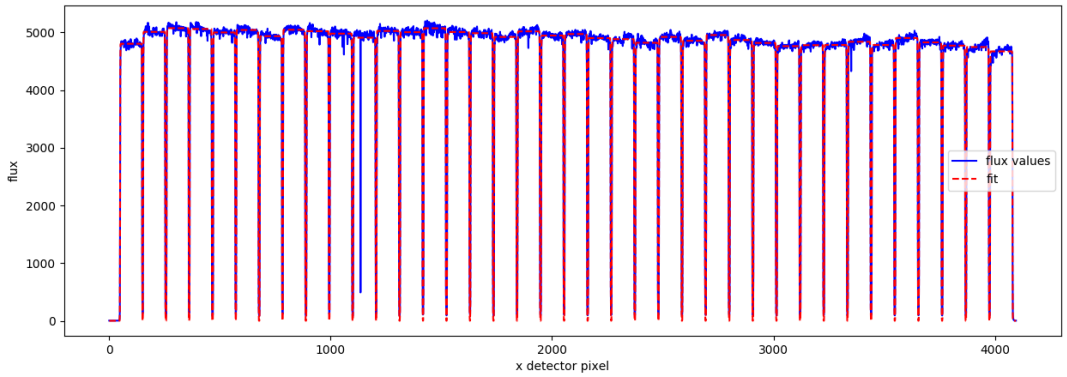

Figure 3. Averaged value along the x-axis of the 100 neighbouring rows around the central row (subfield A for the 20MAS+H setting) and approximate solution solved on it.

The sum of square minimization process is significantly sped-up by the use of the Jacobian of the equation (2). Another advantage of knowing the equation of the solution is to use it to compute the edges coordinates of each slitlet. The edges of a slitlet are defined as the points with a flux equal to a pre-defined ratio of its amplitude. The ratio is by default 5/1000, but it could be specified by the user. The left edge coordinate x_l and the right edge coordinate x_r can be computed by using the inverse of the error function:

$$x_l=\sigma\sqrt{2}erfinv(-1+2ratio)+c-\frac{\Delta}{2} \quad (3)$$

$$x_r=\sigma\sqrt{2}erfinv(1-2ratio)+c+\frac{\Delta}{2} \quad (4)$$

This work is done row by row to estimate the centre and the edges of the slitlets on the whole detector. More precisely, the algorithm implementation works as follow:

1. It computes the averaged value along the x-axis of the 100 neighbouring rows around the central row and it performs a least square minimization on the result to compute the amplitude, the centre and the width of the 38 top-hat profiles corresponding to the slitlets and the standard deviation of the Gaussian profile corresponding to the PSF of the spectrograph.
2. Then it estimates the centres and the edges using a sliding window of then rows in the spectral direction using the same least square minimization. From the estimated top-hat and Gaussian parameters, it computes the left and right coordinates corresponding to a given ratio. The results from step 1 are used as initial parameters. This operation is repeated from the centre towards the top/bottom 10 rows per 10 rows. For more robustness, parameters are initialized using the results computed from the previous group of rows. At the end, the process gives for each slitlet, a list of centres, a list of left edges and a list of right edges detector x-coordinates corresponding to known vertical positions.
3. Because of a possible slitlet overlap, all pixels that are part of two slitlets are excluded: the left edges of a given slitlet are limited by the right edges of the neighbouring slitlet on its left and the right edges are limited by the left edges of the slitlet on its right.
4. Finally, the recipe fits 3 polynomials per slitlet, that give the centre and the left/right edges positions as a function of the detector y-coordinate. The fit eliminates possible deviant positions due to cosmics, bad pixels or other optical effects. Tests done for different instrument settings shows that a polynomial of degree 5 fits accurately the slitlet curvature.
5. The last step consists in computing two polynomials giving the bottom and top edges of each slitlet as a function of the horizontal location of the detector. The edges are traced slitlet per slitlet using Gaussian fitting for each detector column. As done for the vertical edges, the ratio of amplitude is used to determine the slitlet edges.

The polynomials coefficients are saved in FITS table extensions labelled slitlet table. Some statistics on slitlet width and location of midpoint of leftmost and rightmost slitlets of each detector are also saved in the header of this file to track shifts.

3. WAVELENGTH CALIBRATION

The wavelength calibration of HARMONI shall be more accurate than 0.2 pixel RMS. This final accuracy including all the opto-mechanical parts of the instrument, our goal is to determine for the 11 spectral bands, a wavelength-pixel solution more accurate than 0.05 pixel RMS. This solution is computed from exposures obtained with arc lamps illuminating uniformly the focal plane (Figure 4).

Our calibration procedure uses a classical approach, it detects arc lines on the detector and computes the wavelength solution comparing detected lines to an input line catalog. The process is done for each slitlet, the slitlet table previously computed is used to determine the associated detector pixel. Arc lines are detected on the slitlet by using a Gaussian profile fitting. A pattern matching technique (from the CPL library) assigns the corresponding wavelength value from an input line catalog. Then a 2-D polynomial is fitted for each slitlet to compute the final wavelength solution giving the wavelength as a function of the detector coordinates on the slitlet.

The polynomials coefficients are saved in FITS table extensions labeled wavelength calibration table. This files also contains statistics on the detected emission lines (number of lines detected, FWHM of lines detected, quality of the fit ...).

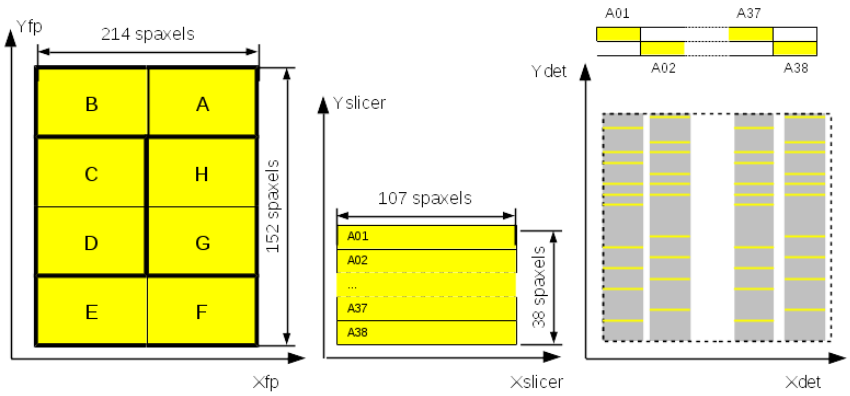

Figure 4. Scheme of an arc exposure through the HARMONI instrument

The accuracy of the wavelength solution depends on the number of lines and their location on the detector which depend on the input lamp but also on the spectral band and on the spectral resolution of the instrument. The HINM has been used to simulate and test different arc exposures for all spectral bands (Figure 5 shows one of these mock data).

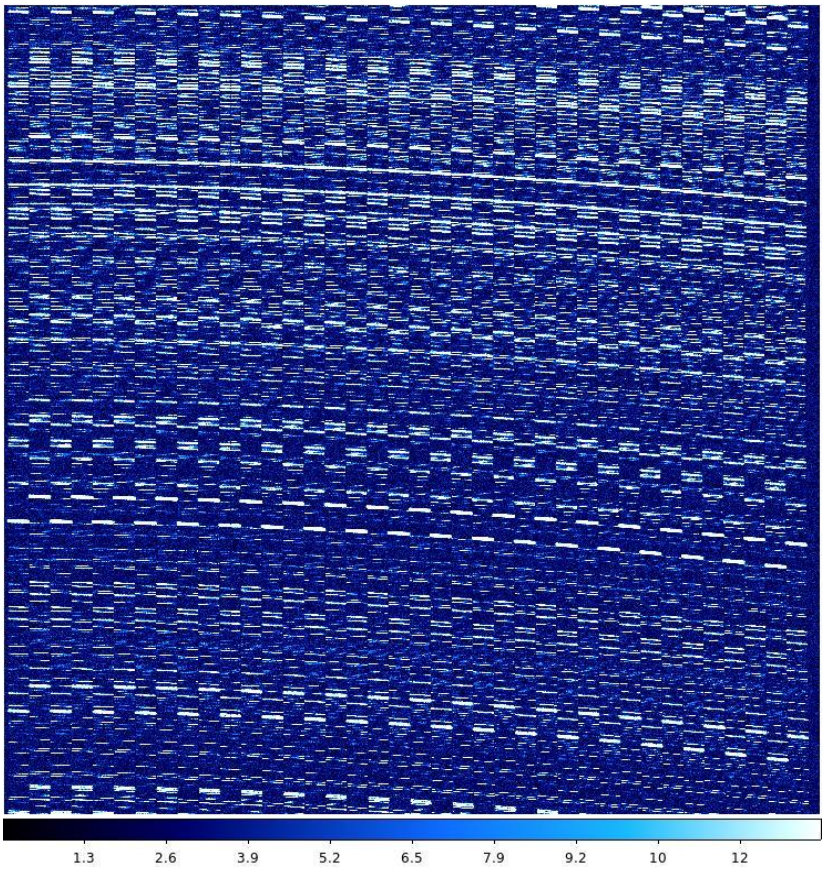

Figure 5. Simulated arc exposure for one detector in H configuration (zscale). FOV uniformly illuminated with a ThAr spectrum.

In order to determine the major parameters of the wavelength calibration, the algorithm has been tested on simulated exposures of arc lines regularly spaced in wavelength. We conclude that:

- A degree 2 along the x-axis and 6 along the y-axis seem to be optimum for the 2D fit polynomials which gives for each slitlet the wavelength as a function of the coordinates on the detector.
- In the case of regular lines with a good S/N and with a perfect knowledge of their wavelength value, we need at minimum 15 lines to reach the accuracy allocated to the pipeline.
- In the case of 15 lines regularly spaced in wavelengths with the same illumination and with a perfect knowledge of their wavelength value, the accuracy of the wavelength calibration remains correct until a S/N>10.

4. RELATIVE LOCATION IN THE FIELD-OF-VIEW

This third recipe computes the transformation between the instrument object focal plane and the detector plane in order to estimate the relative location of each detector pixel in the field-of-view. It takes into account magnification, distortion, misalignment and rotation effects. Residual spatial distortion after calibration in the reconstructed data cube shall be inferior to 0.1 RMS of a spatial resolution element, relative to the input focal plane. This error includes the repeatability error between science and calibration data and the interpolation error, so less than 0.04 pixels RMS are now allocated to the calibration recipe. Due to the required accuracy, the geometrical calibration has been identified as a critical algorithm. The geometrical calibration has to be done for each of the 44 scale/band combinations. To keep the calibration time acceptable, we have developed an advanced algorithm using only two types of exposures, one done with a trace mask and one done with a multi-pinholes mask.

4.1 Geometrical calibration along the x-axis

The geometrical calibration along the x-axis is computed by analyzing the trace mask exposure acquired with a continuum lamp which illuminates a series of slits across the slicing direction (Figure 6). The trace mask has been defined at the Preliminary Design Review (PDR) with seven traces per sub-field with an identifiable pattern to make sure that a vertical trace will not be mistaken with its neighbor in case of a small rotation of the sub-field and/or an important slice misalignment. The width of a trace is around 2 detector pixels which equals to 26µm for the lower spatial case and 199µm for the higher spatial scale. Figure 7 shows a trace exposure simulated with the HINM in the 20MAS scale setting.

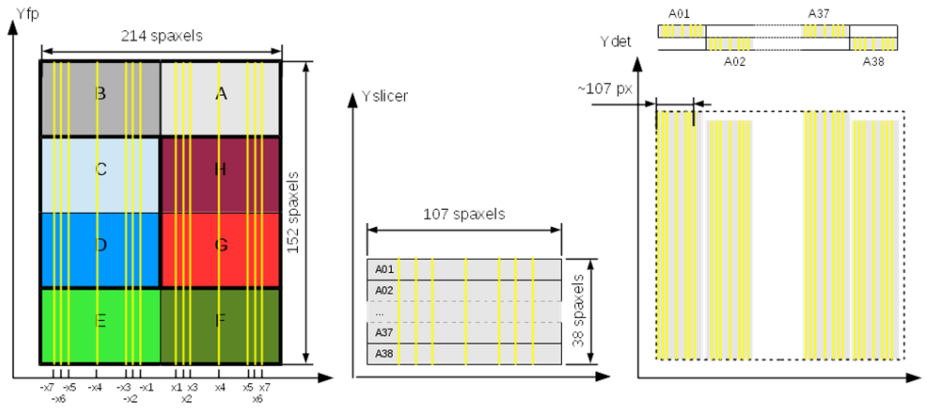

Figure 6. Scheme of a trace exposure through the HARMONI instrument.

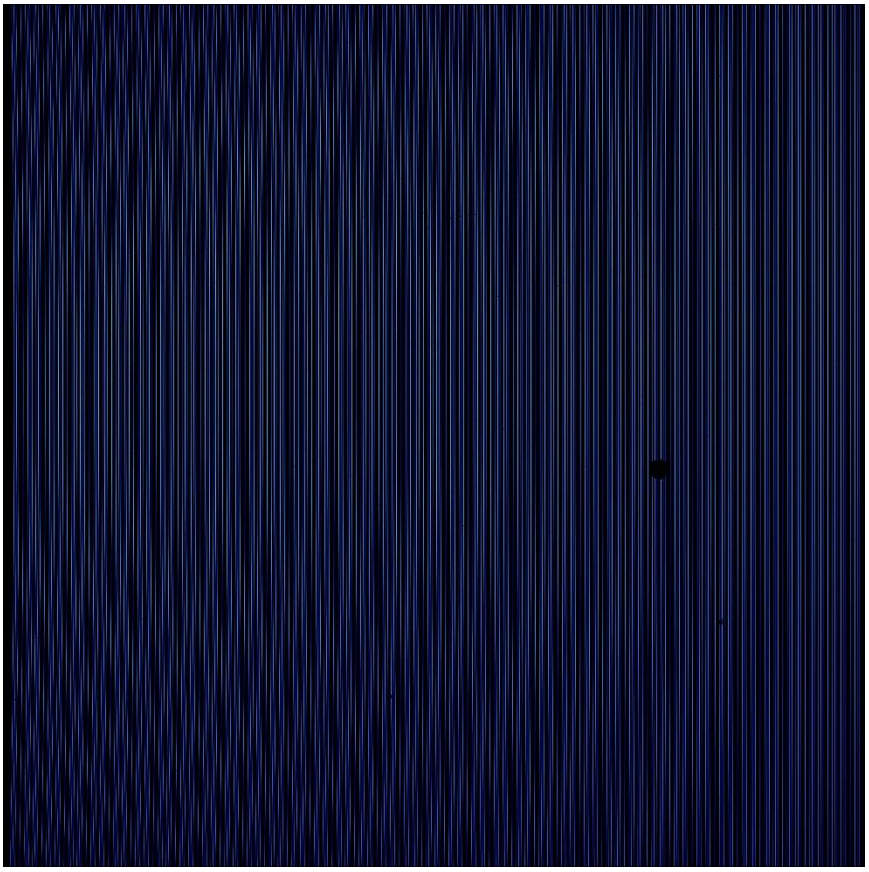

Figure 7. Simulated trace exposure for one detector in 20MAS+H configuration.

The analysis of the trace mask exposures is done independently for each slitlet of each detector. Thus, the algorithm first extracts a sub-image of the detectors pixels of a given slitlet using the slitlet table. This sub-image contains seven spectra given that there are seven traces per sub-field in the mask. The algorithm then determines the position of the seven spectra on the sub-image row by row (along the cross-dispersion). For that, a trace profile is approximated by an analytical Voigt profile, representing a convolution of a Lorentz distribution and a Gaussian distribution. The center of the Voigt profile could be regarded as the location of the maximum flux, the Lorentzian FWHM as the PSF of the instrument without the spectrograph, and the Gaussian FWHM as the PSF of the spectrograph. A collapsed and averaged slitlet row is approximated by the sum of seven Voigt profiles with independent parameters except for the Gaussian. Figure 8 shows the solution found by least-square minimization. The centers of the seven Voigt profiles gives the x-coordinates of the seven spectra for a given detector row.

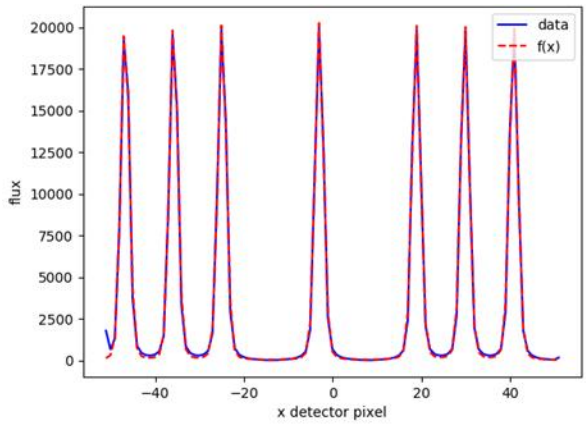

Figure 8. Averaged values along the x-axis of the 100 neighboring rows around the central row (12th slitlet of the subfield A for the 20MAS+H setting) and approximate solution solved on it.

The seven spectra are traced over a slitlet by repeating this minimization along the spectral direction. The process is initialized by performing a first minimization on median flux computed over the 100 central rows and this operation is repeated 10 rows per 10 rows from the centers towards the top/bottom of the slitlet/detector. For more robustness, the fitting parameters are initialized with the results found at the previous position and conditions eliminate outliers when the Voigt amplitude decreases more than 50 percent compared to the previous position or when the error on the center (computed from the covariance matrix estimated during least square minimization) is more than 0.05 pixel. At the end, we obtain the detector coordinates of the seven spectra along the spectral direction.

Then, the wavelength value corresponding to each detector coordinate is computed using the wavelength table and the x-coordinate is corrected from the slice curvature by subtracting the coordinate of the slitlet center given by the slitlet table. Each trace now corresponds to a list of x-coordinates in the slice and a list of wavelength values. As each trace also corresponds to a known x-position in the input focal plane, we fit for each slitlet a 2D polynomial which gives the relative x-coordinate in the instrument focal plane as the function of the wavelength and the position in the slice. This polynomial corrects for the slices misalignments, the slitlet tilt, the sub-field tilt and the sub-field misalignments along the x-axis, the magnification/distortion along the x-axis. Note that this estimation of the x-coordinate uses the trace mask as a reference, assuming traces are orthogonal to the slices. The x-coordinate will be corrected later in order to take into account a possible rotation of the trace mask.

4.2 Geometrical calibration along the y-axis

The geometrical calibration along the Y-axis is estimated by analyzing pinhole mask exposures acquired with a continuum illumination lamp (Figure 9). The diameter of the image of a pinhole is around 3 slices high and not all slices are illuminated. The pinhole mask contains 7x5 pinholes per subfield. Figure 10 shows a pinholes mask exposure simulated with the HINM in the 20MAS scale setting.
As the pinhole diameter is around 3 slices high, most of the flux of the pinhole is spread over three or four slitlets. The flux on these slitlets is used to estimate the y-position of the center of the pinhole in “slice” coordinates. As the analysis is based on the flux, each frame is first corrected for the flat-field through division by the master flat-field.

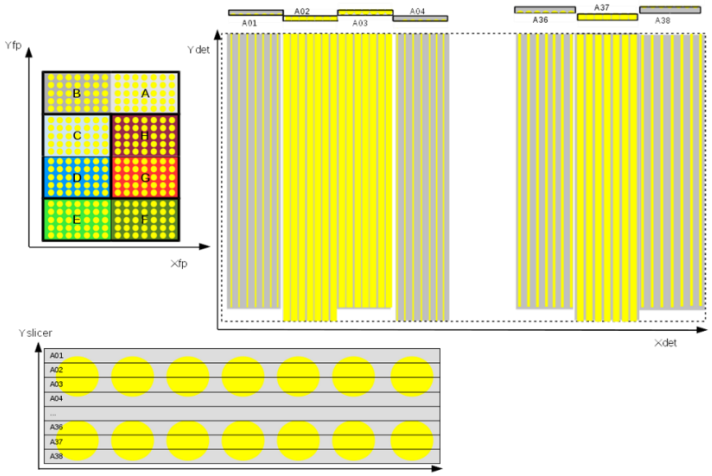

Figure 9. Scheme of a pinholes mask exposure through the HARMONI instrument.

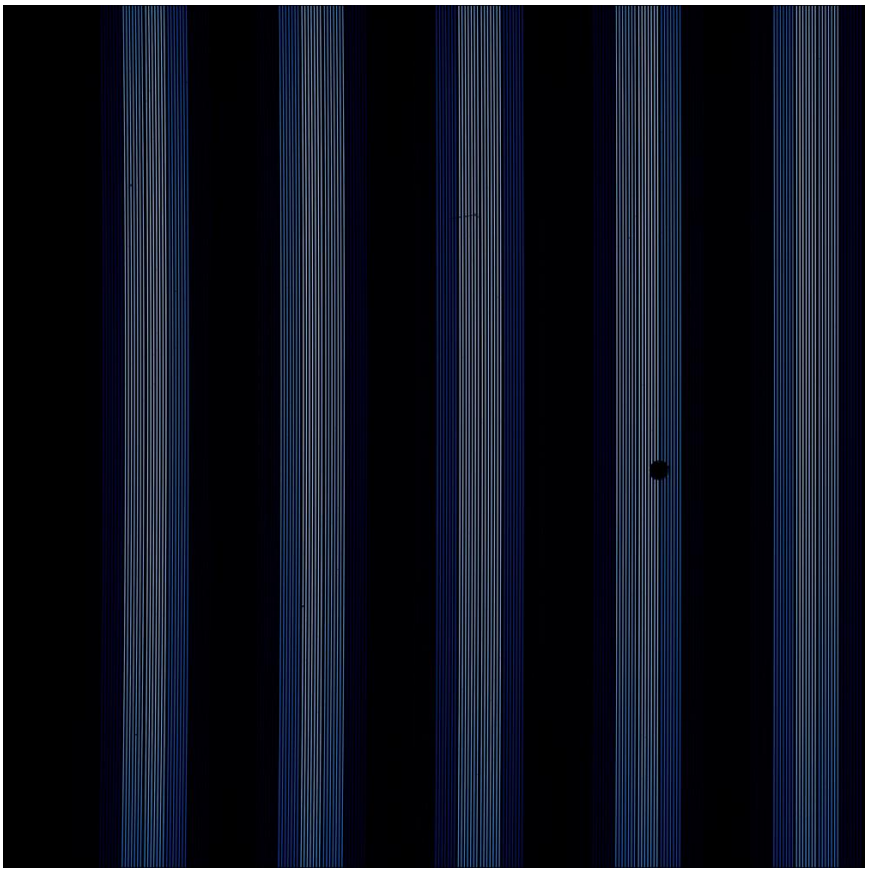

Figure 10. Simulated pinholes mask exposure for one detector in 20MAS+H configuration.

The geometrical calibration along the Y-axis is done independently for each detector. The slitlet and wavelength calibration tables, and the polynomials previously estimated by the analysis of trace exposures are used to assign to each detector pixel:

- a flux value,
- the number of the slitlet in which the pixel belongs (if the pixel is outside all slitlets, it is ignored),
- its wavelength,
- its x-coordinate in the instrument focal plane.

This set of data contains the flux distribution in the slicer plane. Figure 11 shows this flux distribution along the slices and along the x-axis in the instrument focal plane for the subfield A.

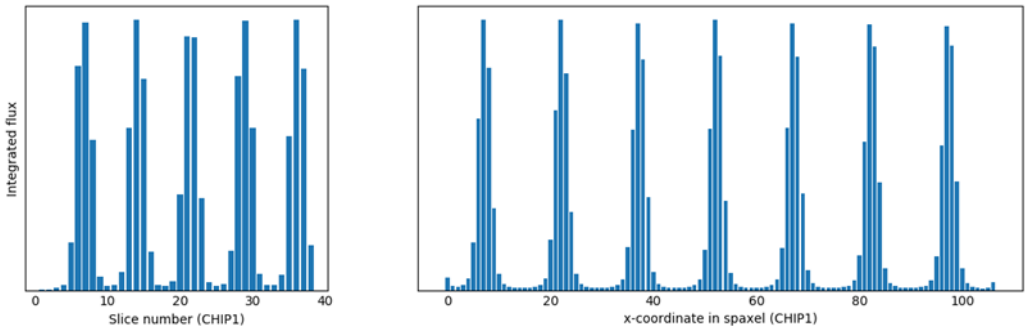

Figure 11. Flux distribution along the slices and along the x-axis for the 20MAS+H configuration.

To locate the pinholes centers on these unstructured 3D data, each pinhole is assimilated to a 2D elliptical Gaussian and we do a global minimization for the 7x5 pinholes of the subfield in order to find the Gaussian parameters $(xc_p, yc_{p,}\sigma x_p, \sigma y_p, I_p)_{p=1,\dots,7x5}$ which minimize the vector:

$$F(x,y) - \sum_{p=1}^{7x5} I_p e^{\frac{-(x-xc_p)^2}{2\sigma x_p{}^2}} e^{\frac{-(y-yc_p)^2}{2\sigma y_p{}^2}}$$

F(x,y) is the flux value of a detector pixel, *x* is the x-coordinate of the detector pixel in the input focal plane, *y* is the number of the slitlet in which the pixel belongs, and I_p is the amplitude, $(xc_p, yc_{p,})$ are center coordinates, $(\sigma x_p, \sigma y_p)$ are standard deviations of the 2D Gaussian simulating the p[th] pinhole.

The least-square minimization is performed on selected pixels in a common wavelength range. For now, we assume here that the chromatism along the y-axis is negligible from the input focal plane to the slicer plane. Note that it will still be possible later to split the analysis in several wavelength steps if we want to characterize a variation along the y-axis. This analysis also assumes that all slices have the same height. According to the slicer specifications, the height of a slice is equal to 1.00 -/+0.01mm. This inaccuracy will affect the estimate of the y-position (1%) but it could be mitigated by taking into account the slice heights if precisely measured after manufacturing.

The minimization gives for each pinhole of the sub-field an estimated y-position in the slicer plane. As we known the position of each pinhole in the input focal plane, we can compute for each subfield the transform between the focal plane and the slicer and correct the subfields misalignments. This transform takes the form of a 2D polynomial that fits the Y transformation.

4.3 Correction of a possible trace mask rotation

The first estimation of the x-coordinate uses the trace mask as a reference, assuming traces are orthogonal to the slices (section 4.1). The analyses of the pinhole mask exposures (section 4.2) give also for each pinhole an accurate estimation

of the x-position in the focal plane which is used to compute a polynomial on the whole field-of-view which corrects for the effect of a possible small rotation of the trace mask.

4.4 Geometry table

The transformation between the instrument object focal plane and the detector plane is estimated in three steps: a first calibration along the x-axis by analyzing the trace mask exposures, a second calibration along the y-axis by analyzing the pinhole mask exposures, and a last correction of the trace mask rotation.

In the same way, the computation of the coordinates of each detector pixel within the instrument object focal plane is done in 3 steps:

1. A first estimation of the x-coordinate is computed from the polynomials estimated for each slitlet by the analysis of trace exposures.
2. The y-coordinate is computed from the polynomial estimated for each detector by the analysis of the pinholes mask exposures.
3. The x-coordinate is corrected from the polynomial valid on the whole field-of-view.

The resulting coordinates are relative coordinates (in mm) in the HARMONI focal plane with the pinhole mask as a reference. The polynomials are saved in a FITS file labelled geometry table.

4.5 Validation

The algorithm has been implemented in Python and tested on exposures simulated by the HINM without AO for 4 different instrument settings chosen to cover the 3 spectral resolutions and the 4 spatial scales. We use a degree 2 along the two axes for the 2D fit polynomials except for the polynomial compensates only for a rotation, one dimension along the two axis is sufficient.

Using the HINM, we generate test exposures from a grid of 14x20+15x21 pinholes in staggered rows. Each pinhole has a diameter corresponding to 2 slices. We pre-process the test mask exposure, detector pixel per detector pixel:

1. The value of the detector is corrected by the master flat
2. The slitlet table is used to determine to which slitlet the pixel belongs to.
3. The wavelength calibration table is used to determine the corresponding wavelength.
4. The geometry table is used to determine its location in the instrument focal plane.

For each pinhole, we select the pixels in a given wavelength range and in a circular-aperture twice larger than the diameter of the pinhole; then we estimate the center of the pinhole by fitting a 2D Gaussian on these pixels and we compare to the expected position.

A first set of tests is done on electron rate maps directly created by the HINM without detector effects. Table 1 summarizes the RMS of the residual spatial distortion after calibration and Figure 12 shows error maps computed on three wavelength ranges for the 20MAS+H configuration. The calibration error along the x-axis is higher and close to the specification (RMS < 0.04). We explain this difference by the fact that it is more impacted by the spectrograph (the spatial sampling is done optically before the spectrograph by the slicer in the y direction and after the spectrograph by the detector in the x direction);

and we have identified small changes for the masks which should improve the accuracy (for example a trace mask pattern with eight lines per sub-field but only one gap).

Table 1.RMS of the residual spatial distortion after calibration

	RMS(spaxel) 4MAS + Khigh	**RMS (spaxel) 10MAS+HK**	**RMS(spaxel) 20MAS+H**	**RMS(spaxel) 60x30mas+IzJ**
Pinholes X-positions accuracy	0.042	0.030	0.034	0.030
Pinholes Y-positions accuracy	0.005	0.007	0.005	0.017

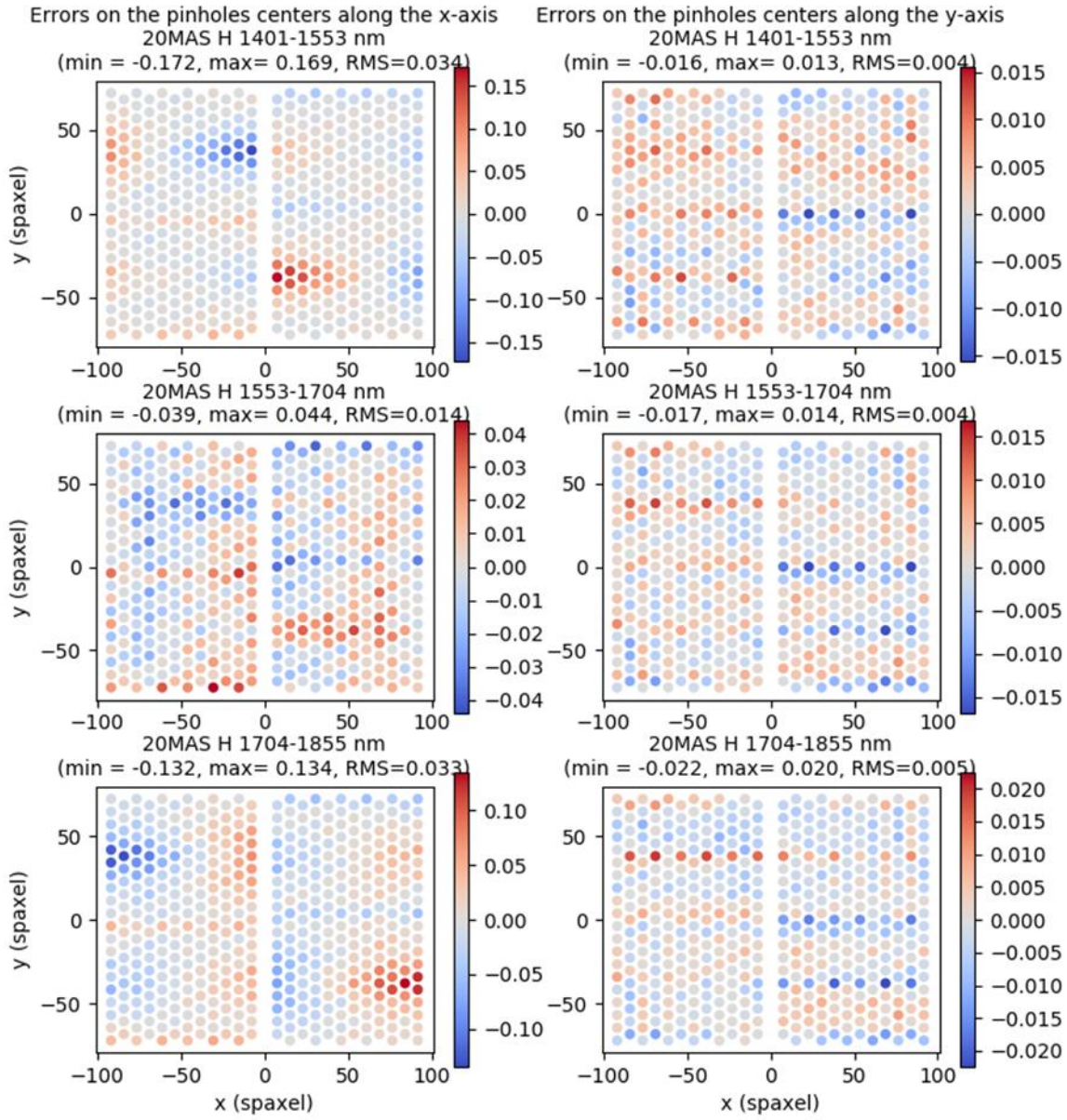

Figure 12. Error maps for three wavelength ranges in 20MAS and H band.

Additional tests on electron rate maps simulated with a rotation of the trace mask or with a slices misalignment confirm that the geometrical calibration properly corrects these optical features (Figure 13). All the test assume that the masks are perfect, or rather that we perfectly known their spatial features. Approximations on location and shape of the traces and

the pinholes could decrease the accuracy of the geometrical calibration. Nevertheless we expect that the average effects on all traces and pinholes will mitigate this problem.

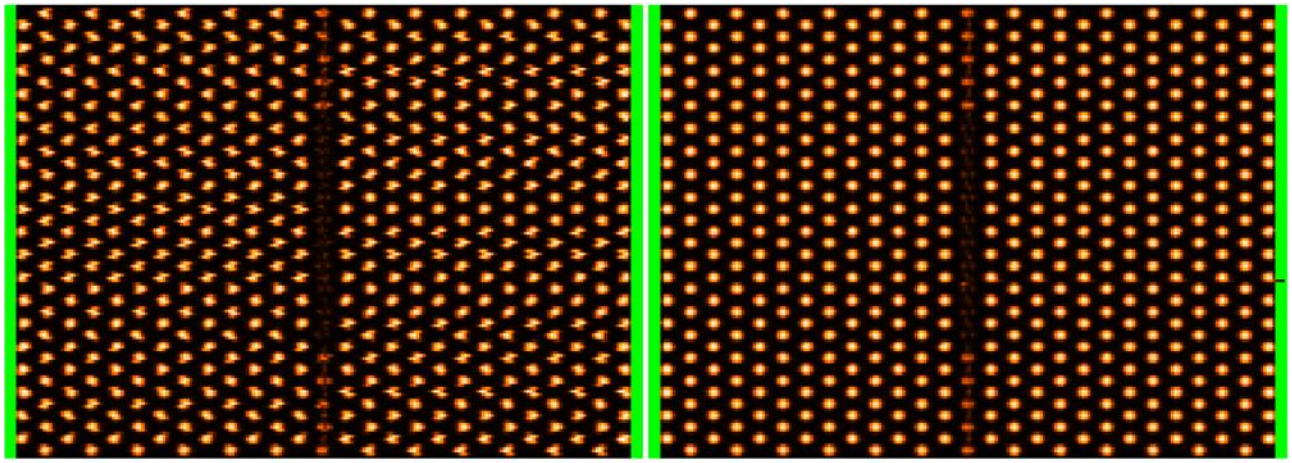

Figure 13.Quick reconstruction of an exposure of the test mask including slice misalignments without (left) and with (right) custom geometry calibration.

Moreover a test done on simulated noisy exposures seems to show that the noise is not affecting the accuracy of the geometrical calibration.

These tests have been performed from exposures from HINM and its simulated calibration module, i.e. with calibration masks in the instrument focal plane. HARMONI also has a similar set of masks inside the cryostat, as part of the pre-optics. Our algorithm will also work with these masks, except that it will not calibrate the effects of the Focal Plane Relay System optics and the cryostat rotation.

5. CONCLUSION

The geometrical calibration provides, for each detector pixel, a wavelength value and a first estimation of the relative pixel coordinates (in mm) in the HARMONI focal plane with the pinhole mask as a reference. It will be followed in the later stages by the computation of the world coordinates RA and DEC, from telescope information and the astrometry table, and by the resampling onto a suitable regular output grid (RA, DEC, λ). The results presented in this article only refer to the knowledge of the relative pixel coordinates. The error on the spatial on-sky coordinates should take into account the interpolation effects and the astrometric calibration error.

Our algorithm emphasizes that the flat calibration, the wavelength calibration and the geometrical calibration form a consistent group: the master flat and the slitlet table are computed from flat exposures, and the wavelength calibration table is computed from arc exposures taken with the same instrument settings and obtained during the same acquisition sequence as the trace and pinholes masks exposures in order to avoid any problem due to the spectra repositioning repeatability.

The proposed algorithm needs to be finalized for the Final Design Review. We have identified changes for the trace mask which should improve the calibration of the relative location along the x-axis. Moreover, the 2D polynomials which fit the transformation along the y-axis must be replaced to 3D polynomials to take into account the chromatic dispersion due to the dichroics in LTAO and SCAO modes. Lastly, it still has to be investigated if some calibration can be shared between spectral ranges or spatial scales.

REFERENCES

[1] Thatte, N. & al., “The E-ELT first light spectrograph HARMONI: capabilities and modes”, Proc. SPIE 9908, 99081X, (2016).

[2] Neichel, B. & al., “HARMONI-first light spectroscopy for the ELT: Getting to the Diffraction limit!”, Proc. SPIE, (2020).

[3] Schnetler, H. & al., “HARMONI-first light spectroscopy for the ELT: The final design of the first diffraction limited 3D spectrograph”, Proc. SPIE, (2020).

[4] Piqueras, L. & al., “ Preliminary design of the HARMONI science software”, Proc. SPIE 9911, 99111Z, (2016).

[5] McKay, D. & al., “The common pipeline library: Standardizing pipeline processing”, Proc. SPIE 5493, (2004).

[6] Modigliani, A. & al., “The High-level Data Reduction Library – A Library for ESO’s Data Reduction Pipelines”, Proc. ADASS(2020).

[7] Jarno, A. & al., “Validating data reduction algorithms through advance instrument simulation-the case of HARMONI”, Proc. ADASS (2020).